1 **Title**

2 Early detection of daylengths with a feedforward circuit coregulated by circadian and diurnal cycles

3

4 **Running title**

5 A dual-cycle circuit detects daylengths

6

7 **Authors**

8 N. Panchy, A. G. von Arnim, T. Hong

Abstract

Light-entrained circadian clocks confer rhythmic dynamics of cellular and molecular activities to animals and plants. These intrinsic clocks allow stable anticipations to light-dark (diel) cycles. Many genes in the model plant *Arabidopsis thaliana* are regulated by diel cycles via pathways independent of the clock, suggesting that the integration of circadian and light signals is important for the fitness of plants. Previous studies of light-clock signal integrations have focused on moderate phase adjustment of the two signals. However, dynamical features of integrations across a broad range of phases remain elusive. We recently found that phosphorylation of RIBOSOMAL PROTEIN OF THE SMALL SUBUNIT 6 (RPS6 or eS6), a ubiquitous post-translational modification across kingdoms, is influenced by the circadian clock and the light-dark (diel) cycle in an opposite manner. In order to understand this striking phenomenon and its underlying information processing capabilities, we built a mathematical model for the eS6-P control circuit. We found that the dynamics of eS6-P can be explained by a feedforward circuit with inputs from both circadian and diel cycles. Furthermore, the early-day response of this circuit with dual rhythmic inputs is sensitive to the changes in daylength, including both transient and gradual changes observed in realistic light intervals across a year, due to weather and seasons. By analyzing published gene expression data, we found that the dynamics produced by the eS6-P control circuit can be observed in the expression profiles of a large number of genes. Our work provides mechanistic insights into the complex dynamics of a ribosomal protein, and it proposes a previously underappreciated function of the circadian clock which not only prepares organisms for normal diel cycles but also helps to detect both transient and seasonal changes with a predictive power.

30 **Statement of Significance**

31 Circadian clocks provide rhythmic dynamics that anticipate light-dark cycles in a consistent fashion. Many
32 genes in plants are controlled by both the circadian clock and light-dark cycles through independent
33 pathways. We built a mathematical model to understand a recent observation that circadian rhythms and
34 light-dark cycles drive the phosphorylation of ribosomal protein eS6 with opposing phases. We found that
35 this phenomenon is governed by a feedforward circuit involving clock and light-dark cycles. With realistic
36 photoperiod data, we show that the circuit can detect both transient (weather) and long-term (seasonal)
37 daylength variations at the beginning of a day, suggesting rich dynamics arising from clock-light signal
38 integration and a new property of the circadian clock in robustly detecting changes in light conditions.

Introduction

Circadian clocks provide animals, plants and certain microbes with rhythmic dynamics. These circadian pacemakers confer fitness advantages to the organisms by establishing stable anticipation of diel light-dark cycles (1, 2) as well as regulating broad morphological changes over the course of the year (3). In the plant model organism *Arabidopsis thaliana (A. thaliana)*, the circadian clock consists of at least four interacting gene modules that form negative feedback loops, which govern an intrinsic oscillator (4, 5). The expression dynamics of several hundred genes in *A. thaliana* are controlled by this circadian oscillator (6, 7). The circadian oscillator retains its essential dynamical features under constant light conditions, reflecting its intrinsic nature (8), but the phase of the oscillations can be adjusted in a process called entrainment by the lights-on signal at dawn (5, 9). In addition, however, the light-dark cycle regulates a large number of genes in a clock-independent fashion (8, 10). Therefore, molecular activities in plants are influenced by at least two periodic signals. Previous studies have found that cellular activities in *A. thaliana*, such as the abundance of the regulator of flowering time CONSTANS (CO) and the cytosolic calcium concentration, require signals from both the clock and the light-dark cycle to regulate timing (i.e. the phase of peak activity) (8, 9, 11). For example, for many mRNA transcripts, the circadian clock leads to a moderate phase shift in the onset or peak time as compared to the light cycle alone (8, 9, 11). However, these paradigms only represent *one* of the many diverse co-regulation modes of clock-light signal integration. It remains unclear whether the integration of circadian and diel light-dark cycles underpins other paradigms of signal processing.

The phosphorylation of RIBOSOMAL PROTEIN OF THE SMALL SUBUNIT 6 (RPS6 or eS6) is a post-translational modification that occurs in a wide range of organisms including animals and plants (12-14). Mice that have only a non-phosphorylatable eS6 show abnormalities at the organismal level (e.g. muscle weakness), indicating that this modification is functionally significant (15). However, while it has been suggested that the eS6 phosphorylation (eS6-P) is implicated in ribosome biogenesis in mammals (12), its

63 biochemical consequence and specific activity, including its molecular role in *A. thaliana*, are largely
64 unknown (13). Interestingly, eS6-P is widely used as a bioreporter for the activity of Target Of Rapamycin
65 (TOR) kinase, a central controller of cell growth and aging (16, 17). We recently found that eS6-P in *A.*
66 *thaliana* is co-regulated by both the circadian clock and the diel cycle, as eS6-P exhibits cycling behavior
67 both in a severely clock-deficient strain and under constant light conditions (18). Unlike other extensively
68 studied cellular processes, eS6-P is controlled by the clock and light-dark cycles in a strikingly opposite
69 manner: in the wild-type strain under constant light the circadian clock drives eS6-P with a peak during
70 the subjective night, whereas in a clock-deficient strain the diel light-dark cycle drives eS6 with a peak
71 during the day (18, 19). However, the biological significance of this remarkable phenomenon at cellular
72 and organismal levels remains elusive.

73 In this study, we constructed a mathematical model to examine the signaling network that regulates eS6-
74 P in *A. thaliana*. We calibrated the model with experimental measurements of the circadian clock and eS6-
75 P under various conditions. We found that the key dynamics of eS6-P can be explained by a feedforward
76 loop that connects the periodic light signals to eS6-P with a direct arm and an indirect arm via the circadian
77 clock. Although this feedforward loop is largely incoherent at the steady state of a symmetrical light-dark
78 cycle (12-hour-light and 12-hour-dark), the amplitude of its output exhibits a high sensitivity to variations
79 in daylength, due to the interaction between the two cyclic components in the loop. Notably, we found a
80 characteristic early day peak of eS6-P that detects and anticipates long days. Furthermore, we combined
81 the model with realistic photoperiod data containing both transient perturbations and long-term
82 variations of light-dark cycles and demonstrated that the detection of daylength variations by this circuit
83 communicates information about changes of both the season and the local environment throughout the
84 year. By comparing our model with several representative competing models with various circuits
85 transmitting only light signals, we found that the robust detection of day length variations requires both
86 the circadian clock and the clock-independent light sensor. Our work demonstrates a remarkable

information processing capacity of a feedforward loop that integrates circadian and light-dark cycles, and it reveals a previously underappreciated role of the circadian clock in anticipating and predicting the changes in light conditions rather than the stable photoperiod.

Results

A mechanistic mathematical model characterizes dynamical features of a feedforward loop controlling eS6-P

To gain a better understanding of the mechanisms underlying the dynamics of eS6-P, we built a mathematical model that includes a light-entrained circadian clock and a light-dependent, clock-independent signaling pathway that regulates the phosphorylation of eS6 (Fig 1A). The latter light-pathway consists of TOR, a kinase that transmits light signals, and ribosomal S6 kinase (S6K), a substrate of TOR (20-23). S6K has been shown to phosphorylate eS6, and the TOR-S6K axis is known as a primary pathway for eS6-P in multiple organisms including plants (17). The clock component of the model is described by four interacting components (LHY/CCA1, the evening complex (EC), PRR9/PRR7, and PRR5/PRR1, denoted as C1, C2, C3 and C4 respectively in this study). It contains the core repressilator of the plant circadian circuit and has previously been used to model the circadian clock (Fig 1A) (4, 24-26). We used this model to capture the essential dynamical features of the clock rather than the molecular details, so we focused on this four-component core repressilator and neglected the additional feedbacks in the clock (4). Because we previously observed that eS6-P oscillates under constant light (18), we also considered clock-driven regulation of eS6 phosphorylation and dephosphorylation in our model (Fig. 1A). Before parameter estimation, each clock component in the model was assumed to regulate (activate or inhibit) the phosphorylation or dephosphorylation of eS6 with unknown parameters. Because we assumed that the clock does not receive signals from the clock-independent pathway or eS6, we first

110 obtained a parameter set for the clock component by fitting the clock model using a qualitative objective
111 function to capture the basic behaviors including cyclic variation in response to light-dark cycles
112 (entrainment) and cycling under constant light conditions (see Methods, Fig. S1). We then compared the
113 simulated clock gene dynamics to previously published expression data (27) to ensure that the model
114 properly represents the phase and shape of the time course measurements (Fig. S2).

115

116 **Fig. 1. Network structure of the eS6-P regulatory circuit and comparisons between simulations and**
117 **experiments. (A)** An influence diagram of a model of the light and clock driven feedforward regulatory
118 system that regulates eS6-P (Clock+Light Model). This model consists of two cycling systems: the light-
119 dark cycle (an oscillatory input) and the circadian clock (an autonomous oscillator). Each cycle regulates
120 cellular processes independently. The regulation by light-dark cycle is mediated by TOR-S6K pathway, and
121 the clock driven regulation is mediated by transcription factors belonging to the LHY/CCA1 (C1), Evening
122 Complex (EC,C2), PRR9/7 (C3), PRR5/1 (C4) modules which contain a repressilator circuit and additional
123 interactions. The light-dark cycle also regulates the circadian clock via the LHY/CCA1 and PRR9/7 modules
124 (entrainment), thus creating a feedforward circuit. Arrows with circle head show influence of unknown
125 directions (positive or negative) before parameter estimation. **(B)** Model predictions (black) and
126 experimental observations (red) of eS6-P under wild-type in long-days (16:8, LD). Error bars indicate
127 standard deviation of pooled measurements at various circadian times. Circadian time is relative to dawn,
128 and regions shaded with grey indicate period of darkness. Blue dots show the raw data points collected
129 prior to pooling over a period of 84 hours (18). **(C)** Model predictions (black) and experimental
130 observations (red) of eS6-P under long-days (16:8, LD) but with a deficient clock (CCA1-overexpression).
131 Error bars indicate standard deviation of pooled measurements at various circadian times. Time is
132 measured and the graph is shaded as in **(B)**. **(D)** Model predictions (black) and experimental observations
133 (red) of eS6-P under constant light. Error bars indicates standard deviation of pooled measurements at

134 various circadian times. Circadian time is measured relative to subjective dawn (Zeitgeber time, ZT) and
135 regions shaded grey indicate periods of subjective night. eS6-P is shown in arbitrary units (a. u.) (see
136 Methods). **(E)** An influence diagram of our model of eS6-P updated with the direction (triangle arrowhead:
137 activation, flat arrowhead: repression). Note that the ambiguous (diamond) regulation of the clock by light
138 reflects that light regulates LHY/CCA1 and PRR9/PRR7 in opposite directions (we assume that light
139 represses CCA1 stability [49], which is important to restrict the LHY/CCA1 peak to dawn). **(F)** An overlay
140 of clock element activities on top of the eS6-P trajectory in wild type under a long-day cycle. The eS6-P
141 cycle is indicated by the solid black curve and the clock components are represented by colored curves
142 (red = C1 = LHY/CCA1, blue = C2 = EC, orange = C3 = PRR9/PRR7 , green = C4 = PRR5/PRR1). Circadian time
143 is measured relative to dawn.

144

145 Next, we fit the Clock+Light model that contains both clock-dependent and clock-independent pathways
146 regulating eS6-P to our recent measurement of eS6-P dynamics under three experimental conditions: a
147 wild-type (WT) strain under long day (LD, 16-hour-light and 8-hour-dark) condition, the WT strain under
148 constant light (LL) condition, and a clock-deficient strain under LD condition (CCA1-overexpression) (18).
149 Using an evolutionary algorithm with a likelihood-based objective function, we found optimized
150 parameter sets that produced trajectories that reasonably matched the experimental data in all three
151 conditions (Fig. 1B-D). Importantly, the model captured the remarkable dynamical features of eS6-P: light
152 alone drives the upregulation of eS6-P during the day (Fig. 1C) whereas the clock alone drives the
153 upregulation of eS6-P during the subjective night (Fig. 1D). Our model also recapitulated the day-peak of
154 the eS6-P when both clock and light-dark cycles are present, suggesting the dominant role of the light-
155 dark cycle. Furthermore, the model predicted a peak of eS6-P shortly after dawn that was not measured
156 experimentally. We found that this observation was not due to the choice of a particular parameter set:
157 the majority of the top 70 (or 5%) models (based on likelihood) from multiple optimization runs generated

158 the same behavior (Fig. S3A). Conversely, the next 70 models lacked the dawn peak, but those models
159 also lacked oscillations under constant light, suggesting a loss of clock regulation (Fig. S3B). Our
160 subsequent analyses are based on the top performing model, which produced a moderate peak of eS6-P
161 after dawn.

162 We next examined how the clock and the light-dark cycles influenced eS6-P mechanistically. While the
163 clock-independent pathway had an obvious mechanism of action, in which the light signal activates a
164 cascade of two kinases that give rise to eS6 phosphorylation, the clock pathway involved a nontrivial
165 combination of molecular influences. We found that eS6-P is regulated by multiple clock-genes that peak
166 at different time points during the day (Fig 1E). Specifically, LHY/CCA1 and PRR9/PRR7 both regulated eS6
167 during the early day with different phases of activity (LHY/CCA1 at dawn and PRR9/PRR7 a few hours after
168 dawn) and opposite effects on eS6 dephosphorylation (LHY/CCA1 inhibits and PRR9/PRR7 promotes
169 dephosphorylation). In contrast, while EC and PRR5/PRR1 also have opposing influences, their activities
170 largely overlapped and canceled each other out. These clock influences collectively resulted in the stably
171 high amount of eS6-P between the early day and dusk, while the early day peak resulted from a
172 coincidence of light, the peak LHY/CCA1 activity, and the absence of peak PRR9/PRR7 activity (Fig 1F). As
173 such, our model showed that at the steady state under LD, the circadian clock and the light-dark cycle
174 influenced eS6-P in a generally opposing manner: during the day, eS6-P is promoted by light but inhibited
175 by PRRs, while during the night, the anticipatory rise of LHY/CCA1 promoted eS6-P prior to dawn, leading
176 both to rapid early rise and the early day peak under normal LD conditions, and the shift in the rise into
177 the subjective night under constant light. Considering the clock's dynamics are light-entrained, the
178 resulting model behaved as a feedforward loop that is largely incoherent at steady state.

179 In conclusion, our calibrated model captured the observed dynamics of eS6-P under multiple conditions,
180 and allowed us to make predictions about the mechanisms underlying these intriguing dynamics. Note
181 that although our discussion primarily focuses on one optimized model, we have reproduced our key

182 conclusions with distributions of parameters rather than a single parameter set (Fig. S3), and with a much
183 more detailed clock model which includes both mRNA and protein concentrations (Fig. S4) (4).

184

185 **Integration of circadian clock and light-sensing pathways detects and anticipates long daylength upon**
186 **transient perturbations of light-dark cycles**

187 We next focused on the dynamics of eS6-P after dawn, when the coincidence of clock and light signals
188 gave rise to a sharp rise and a peak in the model (Fig. 1B-D). We hypothesized that at this key time interval
189 a change in the phase of the lights-on signal significantly affect the dynamics of the model output because
190 the distinct influences of light and clock can synergize with each other depending on their relative phase.
191 We therefore focused on variations in the timing of the transition from night to day (t_{ND}), as they might
192 be used as proxies for transient changes in the local environment (such as weather)or long-term seasonal
193 changes. We ran simulations with the optimized Clock+Light model (Fig. 1E) under the 12-hour-light and
194 12-hour-dark (12L:12D) condition. After the system reached steady state (Day 0), we varied t_{ND} (+/- 4
195 hours) at the start of a single day (Day 1), and tracked the trajectories of eS6-P from the perturbed day
196 and onwards (Fig. 2A). We found that the transient variation of t_{ND} resulted in significant changes in the
197 abundance of eS6-P (response) in the early day, but the responses converged as the day continued. In
198 particular, an early night-to-day transition time ($t_{ND}<0$) gave rise to a higher response including an early
199 day peak, as previously observed with the base model under LD condition (Fig. 1B, Fig. 2B purple), whereas
200 a late transition time ($t_{ND}>0$) had the opposite effect and resulted in a trough (Fig. 2B yellow). In addition,
201 early day maximum eS6-P (defined as the maximum eS6-P over the 4 hours after dawn) varied by as much
202 as 13.8% relative to the case of $\Delta t_{ND} = 0$. We found that the early day peaks (transient responses that are
203 greater than the steady-state response during the day) appeared only when the daylength exceeded 12

204 hours (Fig. 2B cyan). These results show that the eS6-P control circuit detected phase variations of the
205 lights-on signal and thus effectively sensed daylength variation at the beginning of the day.

206

207 **Fig. 2. Response of eS6-P to variations of the night-to-day transition time. (A)** Diagram of perturbations
208 of the night-to-day transition and the effect of daylength relative to a 12-hour-light-12-hour-dark (12L:12D)
209 day. The unperturbed (Δt_{ND} = 0) and perturbed (Δt_{ND} +/- 4 hours) days are labeled. The day period is shown
210 by yellow shaded regions and the maximum extent of the change in daylength is shown by differential
211 shading. The system reached steady state before Day 0. **(B)** Trajectories of eS6-P in response to variations
212 of the night-to-day transition time from Δt_{ND} = -4 (purple) to Δt_{ND} = 4 (yellow) in 0.5-hour increments. All
213 trajectories start at the dusk of the previous day (Day 0, unperturbed), and end at the dusk of the current
214 day (Day 1, perturbed). Dotted lines show trajectories in the absence of light. Thick solid curves show
215 trajectories in the early day (first four hours after dawn), and thin solid curves show trajectories in the
216 remaining hours of the day. Short line segments at the bottom show the time of dawn for each trajectory.
217 **(C)** Side by side plots of clock perturbations in response to varying night to day transition and the resulting
218 effects on eS6-P. For simplicity, we only show the Δt_{ND} = -4 (purple), Δt_{ND} = 0 (red), Δt_{ND} = 4 (yellow) in the
219 bottom figure. In the top panel, color indicates clock factor (red = C1 = LHY/CCA1, blue = C2 = EC, orange
220 = C3 = PRR9/PRR7, green = C4 = PRR5/PRR1), while shade of color represents the timing of dawn (dashed,
221 Δt_{ND} = -4; regular solid, Δt_{ND} = 0; semitransparent solid, Δt_{ND} = 4). Dashed lines show the corresponding
222 times while circles on the clock factors' curves highlight how the ratio between LHY/CCA1 and PRR9/PRR7
223 corresponds to peak height of the response. In all panels, Circadian time is shown in hours relative to
224 normal time of dawn (i.e. +/- 0 hours).

225

226 We found that the sensitivity of eS6-P to changes in the light-dark cycle was associated with the altered
227 relative phase of clock-gene activities with respect to the dawn (Fig. 2C, gray lines) upon perturbations of
228 the light-dark cycle. For example, the earlier dawn allowed synergy between light signal, peak of CCA1/LHY
229 and relatively low activities of PRR modules to give rise to a strong eS6-P response (Fig. 2C). This change
230 of relative phase occurred despite the influence of the transient phase shift on the clock gene dynamics
231 as a form of entrainment (Fig. 2C upper panel). Variation in photoperiod length has been previously shown
232 to affect the absolute phase of circadian genes, altering both their timing relative to dawn and the
233 intervals between peak expression of different circadian genes, with the gap between CCA1/LHY and PRR9
234 growing as the photoperiod becomes longer (26, 28). These results suggest that the circadian clock plays
235 an essential role in the regulation of eS6-P, particularly with regard to its early day dynamics.

236 We therefore asked whether the circadian clock is required for the eS6-P circuit (Fig. 1E, Clock+Light model)
237 to detect long daylength with an early day peak. To this end, we constructed three alternative models
238 that describe various modes in which eS6-P may respond to the light signal in the absence of the clock
239 (Fig. 3A, see Table S2 for parameters). These models are: 1) a linear circuit that transmits light signals to
240 eS6-P (Fig. 3A, top panel), 2) an incoherent feedforward loop (IFFL) that produces an early day peak similar
241 to what the Clock+Light model does under LD condition (Fig. 3A and B, middle panels), and 3) a coherent
242 feedforward loop (CFFL) that allows slow decline of eS6-P upon the withdrawal of light signals (Fig. 3A,
243 lower panel). Note that none of these three models were able to fully fit the observed data (e.g. Fig. 1D)
244 due to the lack of clock regulation. Rather than evaluating these models in terms of their fit to data, we
245 focused on their performance in terms of detecting daylength variations upon dawn.

246

247 **Fig. 3. Response of alternative models of eS6-P circuit to variations of the night to day transition time.**
248 **(A)** Influence diagrams of the three alternative models of eS6-P circuit. In each diagram, the regulatory

factors are indicated by the lettered black circles, and regulatory interactions are denoted by colored lines (blue = activation, red = repression). Right panels show simulation trajectories with these models under the LD condition. Gray regions show the period of night. **(B)** Trajectories of eS6-P in response to variations of the night to day transition time from Δt_{ND} = -4 (purple) to Δt_{ND} = 4 (yellow) in 0.5-hour increments. All trajectories start at the dusk of the previous day (Day 0, unperturbed), and end at the dusk of the current day (Day 1, perturbed). Dotted lines show trajectories in the absence of light. Thick solid curves show trajectories in the early day (first four hours after dawn), and thin solid curves show trajectories in the remaining hours of the day. Short line segments at the bottom show the time of dawn for each trajectory. **(C)** Left: peak metric (ratio of the early day maximum of eS6-P to the eS6-P levels at the dusk) with respect to the perturbations of the daylength. Right: activation time of the eS6-P after dawn with respect to the perturbations of the daylength. Activation time is defined as the time for eS6-P to reach $x_0 + 0.9(x_s - x_0)$, where x_0 is the eS6-P level at the dawn and x_s is the eS6-P level at the dusk.

Each of the three alternative models generated a constant level of eS6-P upon the perturbations of daylength (Fig. 3B cyan). Particularly, the early day peak produced by the IFFL model did not distinguish short and long daylengths (Fig. 3B middle). This insensitivity to daylength variations with the alternative models was reflected in the stable maximum early responses of eS6-P regardless of their ratios to steady state (or end-of-day) eS6-P levels (Fig. 3C left). In addition, we found that the daylength-sensitive early response with the Clock+Light model was anticorrelated with the time for eS6-P to reach its steady state level, e.g. an early dawn accelerated the response of eS6-P (Fig. 3C right). These results suggest that detection of long daylength with early day peaks is a feature that requires the integration of the circadian clock and the clock-independent light-sensing pathway.

271 Because realistic perturbations of daylength may occur through changes of light conditions at both dusk
272 and dawn and on multiple days, we next considered the effects of multiple variations in our simulations.
273 We first allowed -/+ 2 hours of variation in t_{ND} followed by +/-2 hours of variation in the day-to-night
274 transition (t_{DN}) during dusk the previous day (Fig. 4A). Perturbations in each t_{DN}-t_{ND} pair acted in the same
275 direction to either lengthen or shorten the intervening night (Fig. 4A and B, vertical lines). With the
276 Clock+Light model, we found that consecutive changes in dusk and dawn timing gave rise to significant
277 variability in eS6-P response, similar to what was obtained with -/+ 4 hours of t_{ND} alone (Fig. 2B, Fig. 4B
278 and C). Interestingly, +/- 2 hours perturbations of t_{ND} or t_{DN} alone did not generate an early day peak (Fig.
279 4B and C). This suggests that changes in the timing of dusk can be integrated into the eS6-P response by
280 the Clock+Light circuit after dawn and serve as a predicting factor for the current daylength. The
281 incorporation of information in the previous day shows that the Clock+Light circuit can anticipate the
282 daylength changes with a memory capacity.

283 We next examined the effect of changes to t_{ND} on two consecutive days. We observed a slightly increased
284 dynamic range of early eS6-P peak on the second early day compared to the first day with the Clock+Light
285 model (Fig. S5). These results indicate that the Clock+Light circuit was able to detect changes in daylength
286 beyond the altered timing of the current dawn.

287

288 **Fig. 4. Response of eS6-P to variations in night to day transition time following changes of day to night**
289 **transition time the previous dusk. (A)** Diagram of perturbations of the day to night transition and the
290 night to day transition on two consecutive days. The first (perturbed at dusk, Δt_{ND} = -/+ 2 hours) and
291 second days (perturbed at dawn, Δt_{ND} = +/- 2 hours) are labeled. The day period with light is shown by
292 yellow shaded regions and the maximum extent of the change in daylength is shown by differential
293 shading. **(B)** Trajectories of eS6-P in response to variations of the day to night transition time and/or the

night to day transition time from Δt_{ND} = -2, Δt_{DN} = 2 (purple) to Δt_{ND} = 2, Δt_{DN} = -2 (yellow) in 0.25-hour increments. Short line segments at the bottom show the time of dawn or dusk for each trajectory. Upper: dawn perturbation only. Middle: dusk perturbation only. Bottom: both perturbations. **(C)** Peak metric (ratio of the early day (Day 1) maximum of eS6-P to the eS6-P levels at the dusk) with respect to the perturbations of the daylength under various perturbation scenarios.

Integration of circadian clock and light-sensing pathway detects gradual variations of light-dark cycles

We next asked whether the eS6-P circuit responds to progressive, long-term variations of the light-dark cycle, reflective of seasonal changes in the cycle throughout a year. We used a Solar Calculator provided by the National Oceanic and Atmospheric Administration (NOAA) to generate a data set of 'ideal' (i.e. unaffected by transient local changes) daylengths over the course of a year. We simulated the Clock+Light model based on these light-dark cycles for one year at two locations representing the extreme latitudes of the *A. thaliana* distribution, Oslo, Norway, and Praia, Cape Verde (29). As expected from the analysis of transient changes in dawn timing, our model showed a sensitivity of eS6-P to changes in daylength over the year (Fig. 5). The range of eS6-P was correlated with the degree of variation in daylength, which was broader in Oslo (6.2 to 19.0 hours, Fig. 5A) compared to Praia (11.3 to 13.0 hours, Fig. 5B). We observed variations in both the early-day maximum and early-day minimum levels of eS6-P in Oslo (Fig. 5A, orange and pink), with the early-day maxima increasing dramatically as daylength approached its yearly maximum in the summer. Starting from Day 89 of the year, the early-day maxima increased until it reached 148% of the daily steady state at Day 170. As such, we conclude that changes in the daylength over a year are able to the variations in the early-day peak of eS6-P, with the early day maxima exceeding the daily steady state level around 13.5 hours of light. In contrast, much smaller variations of the early-day eS6-P, which never exceeded the daily steady state levels, were observed with the yearly light-dark

317 cycle data in Praia (Fig. 5B), which has a maximum daylength of 13.0 hours. These results suggest that the
318 eS6-P circuit can detect seasonal changes of the light-dark cycles by varying the magnitude of the
319 responses after the dawn and thus is sensitive to changes in daylength even when they occur gradually.

320

321 **Fig. 5. Simulated amounts of eS6-P in response to seasonal changes in daylength over a year. (A)**
322 Simulation of eS6-P over a full year using daylength data for Oslo, Norway (the NOAA Solar Calculator).
323 The left figure shows the eS6-P time course over the full year (gray), overlaid with the early-day maximum
324 (green), early-day minimum (pink), and daily steady state (end-of-day, or dusk) level (black). Peak metric
325 (orange) is defined as the ratio of early-day maximum to the daily steady state level. The right figure shows
326 the eS6-P profiles of individual days selected every two weeks from Day 7 to Day 175 of the year. Time 0
327 is the actual dawn of each day. The color of each curve corresponds to the week number and is correlated
328 with the daylength from short (yellow) to long (purple). Triangles indicate the time at which the end-of-
329 day eS6-P level was measured, and blue dots indicate the position of the early-day peak. **(B)** Simulation of
330 eS6-P across a full year using daylength data for Praia, Cape Verde (the NOAA Solar Calculator). Upper and
331 lower figures are as described in **(A)**. The globe on the left of each panel shows the latitude of the position
332 that the daylength was simulated for.

333

334 We next asked whether the eS6-P circuit can detect changes in light-dark cycles due to transient changes
335 (such as weather) as well as seasonal changes. We obtained a year-long environmental radiometry data
336 from Harvard Forest (30). We normalized the measurement of downward photosynthetic radiation based
337 on the ideal daylength calculations for Boston, Massachusetts from NOAA and obtained a time-series data
338 of realistic light-dark cycles over a year (see Methods). Briefly, a threshold value was used to define
339 day/night with the Harvard Forest data, and the value was chosen to minimize the mean difference

between the inferred hours of daylight and NOAA estimations of daylength. We compared the simulation results for idealized and observed daylength data (Fig. 6) With the idealized daylengths in Boston (9.4 to 15.4 hours), we observed moderate early day peaks in the middle of the year (Fig. 6A). However, transient changes in the observed light data resulted in changes in daylength of up to 1.5 hours, which in turn gave rise to significant variation of early-day peak of eS6-P in response to the changes of sunlight due to daily weather in addition to seasonal changes of sunlight (Fig. 6B). Although transient changes mainly reduced the daylengths from the idealized day lengths throughout the year, there is a significant difference in terms of peak metric between longer (>13 hours) and shorter (<13 hours) days based on the realistic sunlight data (1.01 vs. 0.96. Welch's t-test, $p = 2.7\times10^{-34}$). Furthermore, the absolute difference in early-day peak between idealized and realistic days was greater during longer days (> 13 hours) than during shorter days (< 13 hours) by 10-fold (Welch's t-test, $p = 7.5\times10^{-32}$). As such, these weather induced changes primarily exist in long days, during which the early response of eS6-P is most sensitive to daylength changes. To further illustrate this point, we compared in simulated early day peaks between idealized and realistic days: in both simulations the peak to steady state ratio remained low during short days and increased around a daylength of 13 hours, but the ratios of the two simulations diverged as days grew longer (Fig. 6C). Together, these results show that the eS6-P circuit can detect variations in light-dark cycles when both seasonal and local, transient (weather) changes are considered.

Fig. 6. Simulated amounts of eS6-P in response to transient and seasonal changes in daylength over a year. (A) Simulation of eS6-P across a full year using daylength data for Boston, Massachusetts (the NOAA Solar Calculator). The left figure shows the eS6-P time course over the full year (grey), overlaid with the early-day maximum (green), early-day minimum (pink), and daily steady state (end-of-day, or dusk) level (black). Peak metric (orange) is defined as the ratio of early-day maximum to the daily steady state level. The right figure shows the eS6-P profiles of individual days selected every two weeks from Day 7 to Day

175 of the year. Time 0 is the actual dawn of each day. The color of each curve corresponds to the week number and is correlated with the daylength from short (yellow) to long (purple). Triangles indicate the time at which the end-of-day eS6-P level was measured, and blue dots indicate the position of the early-day peak. **(B)** Simulation of eS6-P over a year using the full year daylength data derived from Harvard Forest radiometry data [26]. The eS6-P time course over the full year (grey) is overlaid with the early-day maximum (green), early-day minimum (pink), and daily steady state (end-of-day, or dusk) level (black). Peak metric (orange) is defined as the ratio of early-day maximum to the daily steady state level. **(C)** The average peak metric (ratio of the early day maximum of eS6-P to the eS6-P levels at the dusk) for NOAA (open circle) and Harvard Forest (closed circle) days binned according to their realistic daylength (every half hour from 8 to 15 hours). Error bars indicate the standard deviation of Harvard Forest days in each bin. The color of the points and bars is correlated with daylength from short (yellow) to long (purple). The globe on the left shows the latitude of the position that the daylength was simulated for.

The sensitivity of early eS6-P responses to daylength variations raises a question whether this detection of daylength variation is robust with respect to fluctuations of light conditions due to, for example, temporary shading by taller plants, and well as fluctuations in molecular concentrations. We therefore introduced high frequency white noise to the variables describing either the amount of transmitted light or eS6-P itself. We used mutual information to quantify the signal transmitted from varied daylength to the early eS6-P response. We found that more than 50% of the mutual information (compared to the noise-free condition with a finite number of bins) was retained (>1 bit) in the presence of significant fluctuations of light or eS6-P (amplitude parameter $\mu = 5$, or about 23% coefficient of variation in light signal) (Fig. S6). This result suggests that the system is robust with respect to the rapid fluctuations of light or molecular concentrations, while it maintains its capacity to detect daylength variations. Intuitively, the peak of eS6-P in long days is driven by a clock-based, slowly increasing trajectory starting from night, and

388 this slow dynamics serves as a signal integration, or averaging method, to reduce the effect of high
389 frequency noise.

390

391 **Dynamical features of the eS6-P circuit represent expression profiles of a large number of genes**

392 Because many genes in *A. thaliana* are co-regulated by the circadian clock and light-dark cycles, we
393 hypothesized that the dynamic features of eS6-P can be observed in the expression patterns of other
394 genes. To identify genes whose expression may resemble the profile of eS6-P, we reanalyzed an *A.*
395 *thaliana* cyclic gene expression data set reported by Dalchau et al. (8), which is based on previously
396 published microarray data with expression patterns of *A. thaliana* genes under LD and LL conditions (6,
397 31, 32). By calculating the phase shift of the peak expression between measurements under LD and LL
398 conditions, we identified 126 genes where peak expression appears in the early day under LD (0-6 hours
399 after dawn) and regressed into the night under LL condition (18-24 hours after dawn), emulating the clock
400 driven sensitivity that we observed in our eS6-P model and the underlying experimental data (see
401 Methods). We next reanalyzed our previously published RNA sequencing data for *A. thaliana* genes under
402 clock-deficient condition (CCA1 overexpression) (10), and further refined the list of 126 genes by selecting
403 those that have peak expression during the day and have significantly higher expression during the day
404 than during the night under the clock-deficient condition (see Methods). With these selection criteria
405 based on the two data sets (Dalchau et al. and Missra et al. (8, 10)), we have identified 92 genes of which
406 time course expression profiles are similar to that of eS6-P (Table S3). As expected, genes identified in this
407 manner exhibited expression patterns qualitatively similar to eS6-P dynamics (Fig. 7).

408

409 **Fig. 7. Genes in *A. thaliana* with eS6-P like expression patterns. (A)** The distribution of the peak phase
410 shift between LD and LL conditions for 92 genes for which phases of expression profiles are similar to

411 those of eS6-P (blue). Equivalent phase shifts for all cyclic genes in the list generated by Dalchau et al. (8)
412 are in gray. **(B-D)** The mRNA expression patterns of 92 genes with phases of expression profiles similar to
413 those of eS6-P for wildtype under LD (B), wildtype under LL (C) and CCA1-overexpression under LD (D)
414 conditions. Time course expression profiles of individual genes are shown as colored curves while the solid
415 black line shows the average expression of all 92 genes. The dotted black line is the average expression
416 pattern of all cyclic genes in the list generated by Dalchau et al. (8). Expression values in all panels were
417 normalized from 0 to 1, such that 0 corresponds to the minimum and 1 correspond to the maximum for
418 each individual gene. **(E)** Distributions of the difference in average mRNA expression level between day
419 and night of 92 eS6-P like genes (blue) and all cyclic genes in the list generated by Dalchau et al. (8) (gray)
420 under CCA1 overexpression condition. Positive values indicate greater average expression during the day
421 and negative values indicate greater average expression during the night.

422

423 Dalchau et al. (8) classified genes with cyclic expression patterns into three categories based on whether
424 the clock or the light-dark cycle dominates the amplitude of the oscillation in mRNA levels: clock-dominant,
425 light-dominant and co-regulated. Note that all three types of genes can be influenced by both the clock
426 and the light-dark cycles, and the category 'co-regulated' here has a more stringent definition in terms of
427 the amplitudes (see Methods). Not surprisingly, the time course profile of eS6-P is categorized as 'co-
428 regulated' based on the definition of Dalchau et al. (see Methods). We found that out of the 92 eS6-P like
429 genes, 66 are classified as 'clock-dominant', while 25 are 'co-regulated' and only 1 is 'light-dominant',
430 suggesting the clock plays a prime role in generating this pattern of expression.

431 We next performed gene ontology (GO) enrichment analysis with the 92 eS6-P like genes using the set of
432 all annotated genes in *A. thaliana* as a background. We found that eS6-P like genes genes are enriched for
433 light response, photosynthetic regulation, and chloroplast localization, as expected from their

434 responsiveness to light (Table S4). Many of the same biological process and cellular compartment terms
435 are also enriched amongst the set of all genes that show cyclic expression patterns (Table S5). However,
436 the enrichment of specific molecular functions regarding memebrane transport (zinc, ferrous iron, and
437 protons) and activities (ATPpase and thioredoxin-disulfide reductase) is unique to eS6-like genes,
438 suggesting they represent a more specialized subset of the light-clock regulated genes. Overall, this
439 suggests that eS6-P like behavior, a photoperiod sensitive shift in peak activity around dawn, is associated
440 with specific light-dependent metabolic functions.

441 These results suggest that the dynamics of eS6-P may represent a broad range of transcriptional, post-
442 transcriptional and post-translational activities in *A. thaliana,* particularly in association with light driven
443 and responsive metabolic functions. While eS6-P is co-regulated by both the light and clock, the phase
444 variation in our model is driven by the clock, and this is consistent with the observation that this pattern
445 is associated with many clock-dominant genes. The similarity of dynamical features among these cellular
446 activities does not indicate a causal relationship, but it raises the possibility that the daylength detection
447 and anticipation features of such dynamics may be used by a large system of molecules in *A. thaliana*. This
448 suggests that the cyclic phosphorylation of eS6 may serve as a key signaling factor or an effector
449 integrating ribosomes into this detection and anticipation system.

450 **Discussion**

451 **Robustness and sensitivity of the clock with respect to light conditions**

452 In this study, we built a mathematical model that describes the dynamics of eS6-P, a ribosomal post-
453 translational modification that occurs in many eukaryotic species. A feedforward regulatory loop connects
454 light signals to eS6-P through a clock dependent pathway and a clock independent pathway. We found
455 that the response of eS6-P is sensitive to the changes of the light-dark cycles, e.g. the daylength variations
456 that are reflected in the time of the dawn. The circuit therefore enables cells to detect and anticipate such
457 variations which may result from changes in season and/or transient changes in weather. We showed that
458 the circadian clock plays important roles in this information processing function. This feature is different
459 from the well-known function of the clock, which ensures robust anticipation of light-dark cycles even
460 under fluctuating light conditions (33, 34). Our study shows that the clock can be used to robustly detect
461 the variations of light conditions at the beginning of a day, which is a function in addition to its traditional
462 role in generating stable rhythmic cues that counteract environmental fluctuations. The circuit achieves
463 this because light and clock signals synergize with each other only at the early phase of the light-dark
464 cycles. This property of the circuit adds to the remarkably diverse ways that the clock may be used by
465 organisms. Furthermore, it might be a fitness advantage for plants to stabilize one group of molecular
466 activities with the clock, while making other activities sensitive to the light conditions using the clock as a
467 reference.

468

469 **Physiological functions of external coincidence**

470 Although the sensitivity of eS6-P to light around dawn has not been investigated comprehensively,
471 experimental data showed that eS6-P rises quickly in response to light (18, 22), as anticipated by our
472 model. The general dynamical feature of eS6-P as a result of clock-light signal integration is consistent

473 with other known signaling events in which the coincidence of internal, clock-derived signals and external
474 light signals drives prominent peaks of molecular activities in plants (8, 9, 35). For example, according to
475 the classic 'external coincidence' mechanism for photoperiodic (seasonal) flowering, the clock drives up
476 the expression of the regulator of flowering, CONSTANS, late in the day. In long-day plants, if CO happens
477 to be exposed to light late in the day, CO is activated and triggers flowering, whereas if CO is met by
478 darkness, as is the case in the winter, flowering remains suppressed (9). Thus, the external coincidence
479 model allows plants to detect variation in photoperiod at the end of the day. Our work suggests another
480 implementation of external coincidence, where variation in light conditions is detected at the beginning
481 of the day by sensing photoperiod sensitive shifts in the phase of circadian genes(26, 28). For CO at the
482 end of the day, coincidence of clock and light signals activates CO while darkness is incoherent with the
483 clock, and represses CO. For comparison, according to our model eS6-P is most sensitive to changes in
484 light conditions at the beginning of the light period because the negative effect of the clock and the
485 potentially positive effect of light are incoherent. We propose that eS6-P helps the plant to sense variation
486 in the onset of light, as a result of cloud cover or shading by other objects in the morning, and adjust its
487 physiology accordingly.

488

489 **Versatile performance objectives of feedforward loops**

490 Previous studies have demonstrated multiple functions of feedforward loops in terms of systems
491 dynamics, including accelerating responses, fold-change detection, adaptation to constant signals and
492 filtering noise (36-39). In addition, it was shown that a feedforward loop can perform a 'counting' function
493 that transforms oscillatory input to stable signals (40). Our study shows a previously underappreciated
494 function of a particular type of feedforward loop containing an intrinsic autonomous oscillator. This
495 system not only detects the phase and period variations of the oscillatory inputs by combining the signals

496 from the external and internal oscillations, but also memorizes the altered response in the following cycles,
497 which may serve to anticipate additional perturbations. The latter feature may be useful for plants to
498 predict weather through encoding the information in the light conditions of the previous day. This result
499 further demonstrates the versatility of the functions of the feedforward loop. Future work is needed to
500 determine whether this phase-detection mechanism can be integrated with other known functions of
501 feedforward loops.

502

503 **Anticipation of changes in environmental conditions**

504 Phosphorylation of eS6 occurs in all organisms where it has been examined, including yeast, plants, and
505 humans (12-14). A previous study showed dramatically increased translation activity in mammalian cells
506 with a phosphorylation-deficient eS6, suggesting a possible role of eS6-P in controlling general resource
507 allocation in cells (15). If this potential function of eS6-P were conserved across kingdoms, then our work
508 would further suggest that eS6-P might tune some aspect of protein synthesis in response to variable light
509 condition. This function, while still to be demonstrated in plants, would not be far-fetched given that
510 translation requires a substantial input in cellular energy, which may be depleted at the end of night. This
511 detection and anticipation of daylength may help plants to prepare for days with particular patterns of
512 light exposures. It has been shown that growing yeast cells can allocate resources to anticipate favorable
513 or unfavorable environmental conditions, and the choice of these anticipations may be made with
514 rhythmic dynamics (41, 42). Regardless of the specific cellular functions of eS6-P, our work sheds light on
515 the rich dynamics of eS6-P under fluctuating environmental conditions. Moreover, the remarkable
516 information processing characteristic of the signaling circuit that controls eS6-P has the capacity to detect
517 and memorize critical cues to allow plants to adapt to a dynamical light environment.

518

Methods

Framework of mathematical models

We modeled gene regulatory networks that control eS6-P using ordinary differential equations (ODEs). The network topologies are shown in Fig. 1. Because most interactions involving high-order molecular interactions, including transcriptional regulation and multisite phosphorylation, we used a generic form of nonlinear ODEs suitable for describing both gene expression and molecular interaction networks (43-46). Each ODE system in the model has the form:

$$\frac{dX_i}{dt} = \gamma_i(F(\sigma_i W_i) - X_i)$$

$$F(\sigma W) = \frac{1}{(1 + e^{-\sigma W})}$$

$$W_i = (\omega_i^o + \sum_j^N \omega_{j\to i} X_j)$$

$$i = 1, \ldots, N \qquad (1)$$

Here, X_i is the activity of protein i. On a time scale $1/\gamma_i$, $X_i(t)$ relaxes toward a value determined by the sigmoidal function, F, which has a steepness set by σ. The basal value of F, in the absence of any influencing factors, is determined by ω_i^0. The coefficients $\omega_{j\to i}$ determine the influence of protein j on protein i. N is the total number of proteins in the network. Activity values are scaled from 0 (absent) to 1 (saturation). For eS6-P, we modeled a single site phosphorylation (S237) that was assumed to be independent of other phosphorylation sites, so we used first order reaction rate law that describes the phosphorylation and dephosphorylation. All variables and parameters are dimensionless. One time unit in the simulations corresponds to approximately 2.53 hours (9.5 unit per cycle), but we transformed the time unit to 1 hour for all subsequent analyses and visualizations.

539 The clock component of our model describes four species (LHY/CCA1, EC, PRR9/7, and PRR5/1), and the
540 light-sensing pathway has two species (TOR and S6K). Together with eS6-P, our full Clock+Light model has
541 seven ODEs in total. Numerical solutions to the ODEs were obtained with Tellurium (47). Computer code
542 for simulating the models under various conditions and reproducing key figures is available at:
543 https://github.com/panchyni/eS6_Models .

544

545 **Parameter estimation**

546 Because the clock component of the model is independent of other elements except for the light input,
547 we first fit the clock components of the model (4 ODEs) by applying qualitative criteria to ensure that it
548 properly replicated features of the circadian clock [18]. We approached optimization the same way as in
549 Locke at al. (5) and De Caluwe et al. (48) by using objective functions which impose costs on deviating from
550 expected, qualitative behavior. Specifically, we penalized the model for (1) having the LHY/CCA1
551 component peak more than 1 hour before or after dawn in long (16L:8D) days, (2) having the same
552 deviation described in (1) in 12L:12D days, (3) having a period under constant light outside of 24 to 25
553 hours, (4) having a period under constant darkness outside of 24 to 28 hours, and (5) having an amplitude
554 of less than 0.1 (i.e. 10% of maximum activity) in any component. These criteria defined by intervals of
555 desired output were used to construct an objective function to evaluate the models. When calculating the
556 objective score, each of the five terms is zero if the output falls in the interval and is the squared difference
557 between the output and the boundary of the interval if the output falls outside the interval. Before
558 optimizing the model parameters, we defined a hyperbox in the parameter space that is bounded by
559 biologically plausible parameter ranges, particularly with regard to the direction of regulation and balance
560 of rates. A population of 40 vectors, each containing 24 parameters, generated by Latin hypercube
561 sampling (LHS), were used as the initial estimation. Starting with this population, we implemented

562 Differential Evolution (DE) optimization algorithm (49, 50) with a mutation rate between 0.35 and 0.65
563 and a crossover rate of between 0.75 and 0.95, and let the optimization run for 15000 generations of DE
564 or the convergence of the evolution. Similar to the approach used by De Caluwe et al. (48), we then
565 compared each component to expression data from Diurnal Database (27) which were normalized onto a
566 0 to 1 scale to ensure the estimated component activity approximated the proper phase and shape of
567 actual clock components (Fig. S2) We performed 250 runs of such optimization to ensure that the
568 performance of the selected parameter set can be reproduced. For fitting eS6-P, we selected among viable
569 models which accurately reflected clock behavior and selected the one with the greatest dynamic range
570 of among the clock components.
571
572 Next, we used the time course measurement of eS6-P to estimate the parameters controlling the
573 regulation of eS6-P by clock components (LHY/CCA1, EC, PRR97, and PRR51 which correspond to C1, C2,
574 C3, and C4 respectively) and the light induced TOR pathway (18). The data set has Western Blot
575 quantification of eS6-P for 78 hours at a 6-hour interval. In the model, the eS6-P variable describes the
576 percentage of the amount of eS6-P with respect to the total eS6. We therefore inferred the fractions of
577 eS6-P from the Western Blot quantification of the experiment and scaled these values based on an
578 approximation of the eS6-P saturation value inferred from Williams et al. (51). 2D-gel electrophoresis data
579 from this study suggest that a majority, but not all eS6 undergoes phosphorylation and that
580 phosphorylation spreads across several sites which may or may not be phosphorylated at the same time
581 (see Fig. 4 and Table 1 in (51)). As the data were not quantified in the original study and estimations based
582 on image analysis were broad (15-77% per site), we chose a conservative estimate of 0.40 as the saturating
583 value. This normalization gives the raw data a range of 0.01 to 0.4 and pooled data (described below) a
584 range of average values from 0.06 to 0.31. This procedure allows us to avoid unrealistic assumptions with
585 either no phosphorylated (eS6-P = 0) or fully phosphorylated (eS6-P = 1) in the system. Because these

586 values are approximate and mainly meant to avoid fitting to unrealistic, extreme values of eS6-P, the
587 model describes eS6-P in arbitrary units (a. u.) rather than actual percentages.

588 We regularized the transformed data by pooling the data points from the same Zeitgeber time, and we
589 used the pooled mean and variance for each time point to calculate the log likelihood. Constant light was
590 emulated in the model by fixing the value of light to 1 and the CCA1 overexpression by fixing the basal
591 production of CCA1 to 50. To examine steady state behavior under each condition, we entrained the
592 model with one day of darkness followed by ten days of the given condition, before comparing the model
593 to the experimental data on the twelfth day. The objective function for the parameter optimization was
594 defined by the log-likelihood function that quantifies the fit of the simulation results to the experimental
595 data with variabilities. Log likelihood estimates for all time points of eS6-P contribute to the objective
596 function equally in an additive manner. As with clock components, we used the DE based optimization
597 algorithm to estimate the remaining parameters. All algorithmic parameters were the same as the
598 optimization for the clock component, expect for the maximum number of generations (5000). We
599 performed 1400 optimization runs, and among the optimized parameter sets we selected the best
600 preforming model with a moderate peak to perform subsequent analyses. Note that the majority of the
601 models in the lowest 5th percentile of likelihood values exhibited the same behavior as the chosen model,
602 including cycling under all three experimental conditions and an early eS6-P peak under LD conditions (Fig.
603 S3A). Models with larger likelihood scores (the next 5 percentiles) show neither this earlier peak nor
604 cycling under constant light (Fig. S3B). A full list of model parameters can be found in Table S1.

605

606 **Applying a detailed clock to our eS6-P model**

607 In addition to our simplified 4-component clock model, we also tested our eS6-P model using a more
608 detailed circadian clock component from De Caluwe et al. (48), which has the same overall network

609 topology but explicitly considers protein and mRNA concentrations (Fig. S4). We added our equation for
610 eS6-P regulation to this full clock model, and used the set of same optimized parameters that we obtained
611 from the simplified model to simulate eS6-P with the light-dark cycle. The CCA1 constitutive
612 overexpression mutant was simulated by removing the clock and light regulated components from the
613 equations for CCA1/LHY transcription (i.e. setting the production rate to maximum). We used the protein
614 concentration of each pair of clock components, representing the mean protein concentration of the two
615 gene products, in place of our generalized clock component activity values. We scaled the concentration
616 values to a range of [0,1] using the minimum and maximum values of that protein pair. However, in the
617 case of CCA1 overexpression, we assumed that the concentration is effectively saturated at the maximum
618 wild-type value, as the average value of CCA1/LHY and PRR9/7 increased by more than five-fold. All
619 parameters for eS6 regulation were the same as in the model in Fig. 1, except for the regulatory effect of
620 the TOR pathway which was increased by 10% to avoid an unrealistic saturation point of eS6-P under wild-
621 type and CCA1 overexpression conditions.

622

623 **Alternative models**

624 To illustrate the unique performance of the Clock+Light model that contains the clock component, we
625 built three alternative models that describe plausible ways in which the eS6-P can transmit the light signal
626 to achieve detection of daylength variations at the beginning of a day. Note that it is trivial for a system
627 to detect daylength variations at the end of a day (e.g. through integration of, or slow response to, light
628 signals), and this detection may not be as useful as the early day detection in terms of anticipating
629 environmental changes. The three alternative models are: 1) a linear circuit that transmits light signals to
630 eS6-P (Fig. 3A, top panel), 2) an incoherent feedforward loop (IFFL) that produces an early day peak similar
631 to what the Clock+Light model does under LD condition (Fig. 3A and B, middle panels), and 3) a coherent

632 feedforward loop (CFFL) that allows slow decline of eS6-P upon the withdrawal of light signals (Fig. 3A,
633 lower panel). Parameter values of these models were manually chosen to give characteristic responses
634 (Fig. 3A, Table S2).

635

636 **Mutual information between daylength variations and eS6-P responses**

637 To examine the transmitted information from daylength variations (signal) to eS6-P abundance (response)
638 when the system is subject to external or internal noise, we introduced uncorrelated multiplicative white
639 noise to ODEs for the light and eS6-P as $dx/dt = f(x_1, x_2, \ldots, x_n) + \mu_x \cdot x \cdot dW$, where dW is a Wiener
640 process that can be discretized as $dW \sim N(0,1) \cdot \sqrt{dt}$ where $N(0,1)$ denotes a normally distributed
641 random variable with zero mean and unit variance, and μ_x represents the amplitude of the fluctuation.
642 To quantify the information transmission, we used mutual information between signal S and response R
643 (52). In the eS6-P system, S represents the perturbation of the time (Δt_{ND}) at which the system receives
644 light signal from a normal light-dark cycle (e.g. 12hr light and 12hr dark), and R represents the eS6-P
645 abundance. The responses were the maximum eS6-P levels in the 4-hour time window after dawn. The
646 calculation of the mutual information was performed with the discretized form (53):

647 $$I(S;R) = -\sum_{i}^{S_B} \frac{k_{s,i}}{N_T} \log \frac{k_{s,i}}{N_T} + \sum_{j}^{R_B} \frac{k_{r,j}}{N_T} \sum_{i}^{S_B} \frac{k_{i,j}}{N_T} \log \frac{k_{i,j}}{N_T} \quad (2)$$

648 Here, signals values were assigned to S_B bins, and the response values were assigned to R_B bins. By
649 binning all signals and responses, we constructed a contingency matrix of which each entry is the number
650 of observations from the simulated data that correspond to that particular signal-response pair. N_T is the
651 sum over all entries in the table, and $k_{i,j}$ is the number of instances of signal i that resulted in response j.
652 In this study, 21 signal bins and 10 response bins were used. Using more response or signal bins will likely
653 increase the mutual information, so our analysis focuses on comparisons of lower bounds of the mutual

information. The bounds of the response bins were determined by the minimal and maximal responses in the absence of the noise. For each signal value, 200 simulations were performed.

Photoperiod data processing

We obtained a copy of the NOAA Solar Calculator (https://www.esrl.noaa.gov/gmd/grad/solcalc/calcdetails.html) and generated approximated day length information (i.e. Sunlight Duration) for a full year for three locations: Oslo, Norway (59.91 Latitude, 110.75 Longitude), Praia, Cape Verde (14.92 Latitude, -23.51 Longitude), and Boston, Massachusetts (42.35 Latitude, -71.05 Longitude). For inclusion in our model, we fit a model of day-night variation to each data set with the following form:

$$L = a + b \cdot \sin\left(\frac{2\pi d}{365} - c\pi\right) + \sin\left(\frac{2\pi t}{T}\right) \tag{3}$$

where the rightmost sine term represents a base 12-hr light/dark cycles and the leftmost sine term modulates this average day based on the time of the year. Here, d is the day of the year, t is the time of day in hours and T is the period of the day in hours. The parameters a, b, and c, are fit such that the fraction of daylight ($L > 0$) conforms to the NOAA estimations for each day (values for each location are listed in Table S6). With this idealized year-long data, the time for analysis of daily response is based the natural light condition rather than any artificially defined time. We also obtained measurement of radiation data in the Harvard Forest (30) including downward oriented photosynthetically active radiation (par.down), which we used as an approximation for daylight. A threshold value (9.0) was used to define day/night using par.down and was chosen such that it minimized the average difference between the inferred hours of daylight and NOAA estimations of day length across all days binned by month. For inclusion in our model, we smoothed radiation data from 2006 (which had the fewest missing values) using cubic splines and applied the threshold to generate binary day/night values.

676

677 **Identification of genes with time-series expression profiles similar to eS6-P dynamics**

678 To identify genes that show similar cyclic patterns to eS6-P dynamics under LD, LL and CCA1
679 overexpression conditions, we first selected genes identified by Dalchau et al. (8) where the peak
680 expression in long-day was during the early day (ZT 0-6 hours) but the peak expression in constant light
681 was during subjective night (ZT 18-24 hours). There were 126 genes that satisfy these conditions. We then
682 used the RNA sequencing data from Missra et al. (measurement under CCA1 overexpression condition) to
683 further filter these genes. We selected genes that had both peak expression during the day, and a
684 difference between average expression during the day and night of at least 25% of the peak value under
685 CCA1 overexpression condition. To visualize the time course profiles of these genes, we used data from
686 Diurnal Database for LD (27), Edwards et al. for LL (32), and Missra et al. for CCA1 overexpression (10).

687 For gene ontology (GO) analysis, we used all 92 eS6-P like genes and tested for enrichment against all *A.*
688 *thaliana* genes using PANTHER ((54); available through http://geneontology.org/). The same procedure
689 we used when testing all genes identified by Dalchau et al.(8). *p*-values were calculated using the Fisher's
690 exact test and multiple test correction was done using Benjamini-Hochberg method with a false discovery
691 rate threshold of 0.05.

692 Dalchau et al. classified the genes with cyclic expression patterns into three categories: light-dominant,
693 clock dominant and co-regulated (8). To examine which category the eS6-P profile would belong to, we
694 used the same approach to classifying light/clock regulation as Dalchau et al. by comparing the ratio of
695 eS6-P amplitude driven by the clock (constant light) to that driven by the light-dark cycle. Briefly,
696 amplitude difference between LL condition and LD condition was used to determine whether light or clock
697 dominates the regulation of each gene. With our eS6-P data, the amplitude under the LD condition is
698 higher than that under LL condition by 2.17 fold (difference in Bode magnitude = -3.3 decibels, dB), which

categorizes eS6 phosphorylation as a process co-regulated by light and clock according to the cutoffs (±7dB difference in Bode magnitude), although light regulation is favored.

Author Contributions

Designed research: TH. Performed research: NP and TH. Analyzed data and wrote the manuscript: NP, AGV and TH.

Conflict of Interest

The authors declare no conflict of interest.

710 **References**

711 1. Dodd, A. N., N. Salathia, A. Hall, E. Kévei, R. Tóth, F. Nagy, J. M. Hibberd, A. J. Millar, and A. A. R.
712 Webb. 2005. Plant circadian clocks increase photosynthesis, growth, survival, and competitive
713 advantage. Science 309(5734):630-633.

714 2. Turek, F. W., C. Joshu, A. Kohsaka, E. Lin, G. Ivanova, E. McDearmon, A. Laposky, S. Losee-Olson, A.
715 Easton, and D. R. Jensen. 2005. Obesity and metabolic syndrome in circadian Clock mutant mice.
716 Science 308(5724):1043-1045.

717 3. Shim, J. S., A. Kubota, and T. Imaizumi. 2017. Circadian clock and photoperiodic flowering in
718 Arabidopsis: CONSTANS is a hub for signal integration. Plant Physiol. 173(1):5-15.

719 4. Pokhilko, A., A. P. Fernández, K. D. Edwards, M. M. Southern, K. J. Halliday, and A. J. Millar. 2012. The
720 clock gene circuit in Arabidopsis includes a repressilator with additional feedback loops. Mol. Syst.
721 Biol. 8(1).

722 5. Locke, J. C. W., L. Kozma-Bognár, P. D. Gould, B. Fehér, E. Kevei, F. Nagy, M. S. Turner, A. Hall, and A.
723 J. Millar. 2006. Experimental validation of a predicted feedback loop in the multi-oscillator clock of
724 Arabidopsis thaliana. Mol. Syst. Biol. 2(1).

725 6. Harmer, S. L., J. B. Hogenesch, M. Straume, H.-S. Chang, B. Han, T. Zhu, X. Wang, J. A. Kreps, and S. A.
726 Kay. 2000. Orchestrated transcription of key pathways in Arabidopsis by the circadian clock. Science
727 290(5499):2110-2113.

728 7. Michael, T. P., T. C. Mockler, G. Breton, C. McEntee, A. Byer, J. D. Trout, S. P. Hazen, R. Shen, H. D.
729 Priest, and C. M. Sullivan. 2008. Network discovery pipeline elucidates conserved time-of-day–
730 specific cis-regulatory modules. PLoS Genet. 4(2).

731 8. Dalchau, N., K. E. Hubbard, F. C. Robertson, C. T. Hotta, H. M. Briggs, G.-B. Stan, J. M. Gonçalves, and
732 A. A. R. Webb. 2010. Correct biological timing in Arabidopsis requires multiple light-signaling
733 pathways. Proc. Natl. Acad Sci. U. S. A. 107(29):13171-13176.

734 9. Salazar, J. D., T. Saithong, P. E. Brown, J. Foreman, J. C. W. Locke, K. J. Halliday, I. A. Carré, D. A. Rand,
735 and A. J. Millar. 2009. Prediction of photoperiodic regulators from quantitative gene circuit models.
736 Cell 139(6):1170-1179.

737 10. Missra, A., B. Ernest, T. Lohoff, Q. Jia, J. Satterlee, K. Ke, and A. G. von Arnim. 2015. The circadian
738 clock modulates global daily cycles of mRNA ribosome loading. The Plant Cell 27(9):2582-2599.

739 11. Xu, X., C. T. Hotta, A. N. Dodd, J. Love, R. Sharrock, Y. W. Lee, Q. Xie, C. H. Johnson, and A. A. R. Webb.
740 2007. Distinct light and clock modulation of cytosolic free Ca2+ oscillations and rhythmic
741 CHLOROPHYLL A/B BINDING PROTEIN2 promoter activity in Arabidopsis. The Plant Cell 19(11):3474-
742 3490.

743 12. Chauvin, C., V. Koka, A. Nouschi, V. Mieulet, C. Hoareau-Aveilla, A. Dreazen, N. Cagnard, W.
744 Carpentier, T. Kiss, and O. Meyuhas. 2014. Ribosomal protein S6 kinase activity controls the ribosome
745 biogenesis transcriptional program. Oncogene 33(4):474.

746 13.Meyuhas, O. 2015. Ribosomal protein S6 phosphorylation: four decades of research. Int. Rev. Cell
747 Mol. Biol. Elsevier, pp. 41-73.

748 14.Yerlikaya, S., M. Meusburger, R. Kumari, A. Huber, D. Anrather, M. Costanzo, C. Boone, G. Ammerer,
749 P. V. Baranov, and R. Loewith. 2016. TORC1 and TORC2 work together to regulate ribosomal protein
750 S6 phosphorylation in Saccharomyces cerevisiae. Mol. Biol. Cell 27(2):397-409.

751 15.Ruvinsky, I., M. Katz, A. Dreazen, Y. Gielchinsky, A. Saada, N. Freedman, E. Mishani, G. Zimmerman, J.
752 Kasir, and O. Meyuhas. 2009. Mice deficient in ribosomal protein S6 phosphorylation suffer from
753 muscle weakness that reflects a growth defect and energy deficit. PLoS One 4(5):e5618.

754 16.Biever, A., E. Valjent, and E. Puighermanal. 2015. Ribosomal protein S6 phosphorylation in the
755 nervous system: from regulation to function. Front. Mol. Neurosci. 8:75.

756 17.Dobrenel, T., E. Mancera-Martinez, C. Forzani, M. Azzopardi, M. Davanture, M. Moreau, M.
757 Schepetilnikov, J. Chicher, O. Langella, and M. Zivy. 2016. The Arabidopsis TOR kinase specifically
758 regulates the expression of nuclear genes coding for plastidic ribosomal proteins and the
759 phosphorylation of the cytosolic ribosomal protein S6. Frontiers in plant science 7:1611.

760 18.Enganti, R., S. K. Cho, J. D. Toperzer, R. A. Urquidi-Camacho, O. S. Cakir, A. P. Ray, P. E. Abraham, R. L.
761 Hettich, and A. G. von Arnim. 2018. Phosphorylation of ribosomal protein RPS6 integrates light
762 signals and circadian clock signals. Frontiers in plant science 8:2210.

763 19.Choudhary, M. K., Y. Nomura, L. Wang, H. Nakagami, and D. E. Somers. 2015. Quantitative circadian
764 phosphoproteomic analysis of Arabidopsis reveals extensive clock control of key components in
765 physiological, metabolic, and signaling pathways. Mol. Cell. Proteomics 14(8):2243-2260.

766 20.Magnuson, B., B. Ekim, and D. C. Fingar. 2012. Regulation and function of ribosomal protein S6 kinase
767 (S6K) within mTOR signalling networks. Biochem. J. 441(1):1-21.

768 21.Schmelzle, T., and M. N. Hall. 2000. TOR, a central controller of cell growth. Cell 103(2):253-262.

769 22.Chen, G.-H., M.-J. Liu, Y. Xiong, J. Sheen, and S.-H. Wu. 2018. TOR and RPS6 transmit light signals to
770 enhance protein translation in deetiolating Arabidopsis seedlings. Proc. Natl. Acad Sci. U. S. A.
771 115(50):12823.

772 23.Pfeiffer, A., D. Janocha, Y. Dong, A. Medzihradszky, S. Schöne, G. Daum, T. Suzaki, J. Forner, T.
773 Langenecker, and E. Rempel. 2016. Integration of light and metabolic signals for stem cell activation
774 at the shoot apical meristem. Elife 5:e17023.

775 24.Bujdoso, N., and S. J. Davis. 2013. Mathematical modeling of an oscillating gene circuit to unravel the
776 circadian clock network of Arabidopsis thaliana. Frontiers in Plant Science 4:3.

777 25.Avello, P. A., S. J. Davis, J. Ronald, and J. W. Pitchford. 2019. Heat the Clock: Entrainment and
778 Compensation in Arabidopsis Circadian Rhythms. Journal of circadian rhythms 17.

779 26.Fogelmark, K., and C. Troein. 2014. Rethinking transcriptional activation in the Arabidopsis circadian
780 clock. PLoS Comput. Biol. 10(7).

781 27.Mockler, T. C., T. P. Michael, H. D. Priest, R. Shen, C. M. Sullivan, S. A. Givan, C. McEntee, S. A. Kay,
782 and J. Chory. 2007. The DIURNAL project: DIURNAL and circadian expression profiling, model-based
783 pattern matching, and promoter analysis. Cold Spring Harb. Symp. Quant. Biol. 72:353-363.

784 28.Webb, A. A. R., M. Seki, A. Satake, and C. Caldana. 2019. Continuous dynamic adjustment of the plant
785 circadian oscillator. Nature communications 10(1):1-9.

786 29.Weigel, D. 2012. Natural variation in Arabidopsis: from molecular genetics to ecological genomics.
787 Plant Physiol. 158(1):2-22.

788 30.Moore, K. E., D. R. Fitzjarrald, R. K. Sakai, M. L. Goulden, J. W. Munger, and S. C. Wofsy. 1996.
789 Seasonal variation in radiative and turbulent exchange at a deciduous forest in central
790 Massachusetts. Journal of Applied Meteorology 35(1):122-134.

791 31.Yanovsky, M. J., and S. A. Kay. 2002. Molecular basis of seasonal time measurement in Arabidopsis.
792 Nature 419(6904):308.

793 32.Edwards, K. D., P. E. Anderson, A. Hall, N. S. Salathia, J. C. W. Locke, J. R. Lynn, M. Straume, J. Q.
794 Smith, and A. J. Millar. 2006. FLOWERING LOCUS C mediates natural variation in the high-
795 temperature response of the Arabidopsis circadian clock. The Plant Cell 18(3):639-650.

796 33.Troein, C., J. C. W. Locke, M. S. Turner, and A. J. Millar. 2009. Weather and seasons together demand
797 complex biological clocks. Curr. Biol. 19(22):1961-1964.

798 34.Gonze, D., J. Halloy, and A. Goldbeter. 2002. Robustness of circadian rhythms with respect to
799 molecular noise. Proc. Natl. Acad Sci. U. S. A. 99(2):673-678.

800 35.Seaton, D. D., A. Graf, K. Baerenfaller, M. Stitt, A. J. Millar, and W. Gruissem. 2018. Photoperiodic
801 control of the Arabidopsis proteome reveals a translational coincidence mechanism. Mol. Syst. Biol.
802 14(3).

803 36.Mangan, S., S. Itzkovitz, A. Zaslaver, and U. Alon. 2006. The incoherent feed-forward loop accelerates
804 the response-time of the gal system of Escherichia coli. J. Mol. Biol. 356(5):1073-1081.

805 37.Ghosh, B., R. Karmakar, and I. Bose. 2005. Noise characteristics of feed forward loops. Phys. Biol.
806 2(1):36.

807 38.Mangan, S., and U. Alon. 2003. Structure and function of the feed-forward loop network motif. Proc.
808 Natl. Acad Sci. U. S. A. 100(21):11980-11985.

809 39.Goentoro, L., O. Shoval, M. W. Kirschner, and U. Alon. 2009. The incoherent feedforward loop can
810 provide fold-change detection in gene regulation. Mol. Cell 36(5):894-899.

811 40.Zhang, C., R. Tsoi, F. Wu, and L. You. 2016. Processing oscillatory signals by incoherent feedforward
812 loops. PLoS Comput. Biol. 12(9):e1005101.

813 41.Gurvich, Y., D. Leshkowitz, and N. Barkai. 2017. Dual role of starvation signaling in promoting growth
814 and recovery. PLoS Biol. 15(12):e2002039.

42. Metzl-Raz, E., M. Kafri, G. Yaakov, I. Soifer, Y. Gurvich, and N. Barkai. 2017. Principles of cellular resource allocation revealed by condition-dependent proteome profiling. Elife 6.

43. Watanabe, K., N. Panchy, S. Noguchi, H. Suzuki, and T. Hong. 2019. Combinatorial perturbation analysis reveals divergent regulations of mesenchymal genes during epithelial-to-mesenchymal transition. npj Syst Biol Appl 5(1):21.

44. Hong, T., J. Xing, L. Li, and J. J. Tyson. 2012. A simple theoretical framework for understanding heterogeneous differentiation of CD4+ T cells. BMC Syst. Biol. 6(1):66-66.

45. Hong, T., J. Xing, L. Li, and J. J. Tyson. 2011. A Mathematical Model for the Reciprocal Differentiation of T Helper 17 Cells and Induced Regulatory T Cells. PLoS Comput. Biol. 7(7):e1002122-e1002122.

46. Mjolsness, E., D. H. Sharp, and J. Reinitz. 1991. A connectionist model of development. J. Theor. Biol. 152(4):429-453.

47. Choi, K., J. K. Medley, M. König, K. Stocking, L. Smith, S. Gu, and H. M. Sauro. 2018. Tellurium: an extensible python-based modeling environment for systems and synthetic biology. Biosystems 171:74-79.

48. De Caluwé, J., Q. Xiao, C. Hermans, N. Verbruggen, J.-C. Leloup, and D. Gonze. 2016. A compact model for the complex plant circadian clock. Frontiers in plant science 7:74.

49. Hong, T., C. Oguz, and J. J. Tyson. 2015. A Mathematical Framework for Understanding Four-Dimensional Heterogeneous Differentiation of CD4+ T Cells. Bull. Math. Biol.:1-19.

50. Ye, Y., X. Kang, J. Bailey, C. Li, and T. Hong. 2019. An enriched network motif family regulates multistep cell fate transitions with restricted reversibility. PLoS Comput. Biol. 15(3):e1006855.

51. Williams, A. J., J. Werner-Fraczek, I. F. Chang, and J. Bailey-Serres. 2003. Regulated phosphorylation of 40S ribosomal protein S6 in root tips of maize. Plant Physiol. 132(4):2086-2097.

52. Shannon, C. E. 1948. A mathematical theory of communication. Bell system technical journal 27(3):379-423.

53. Cheong, R., A. Rhee, C. J. Wang, I. Nemenman, and A. Levchenko. 2011. Information transduction capacity of noisy biochemical signaling networks. Science 334(6054):354-358.

54. Mi, H., A. Muruganujan, J. T. Casagrande, and P. D. Thomas. 2013. Large-scale gene function analysis with the PANTHER classification system. Nat. Protoc. 8(8):1551.

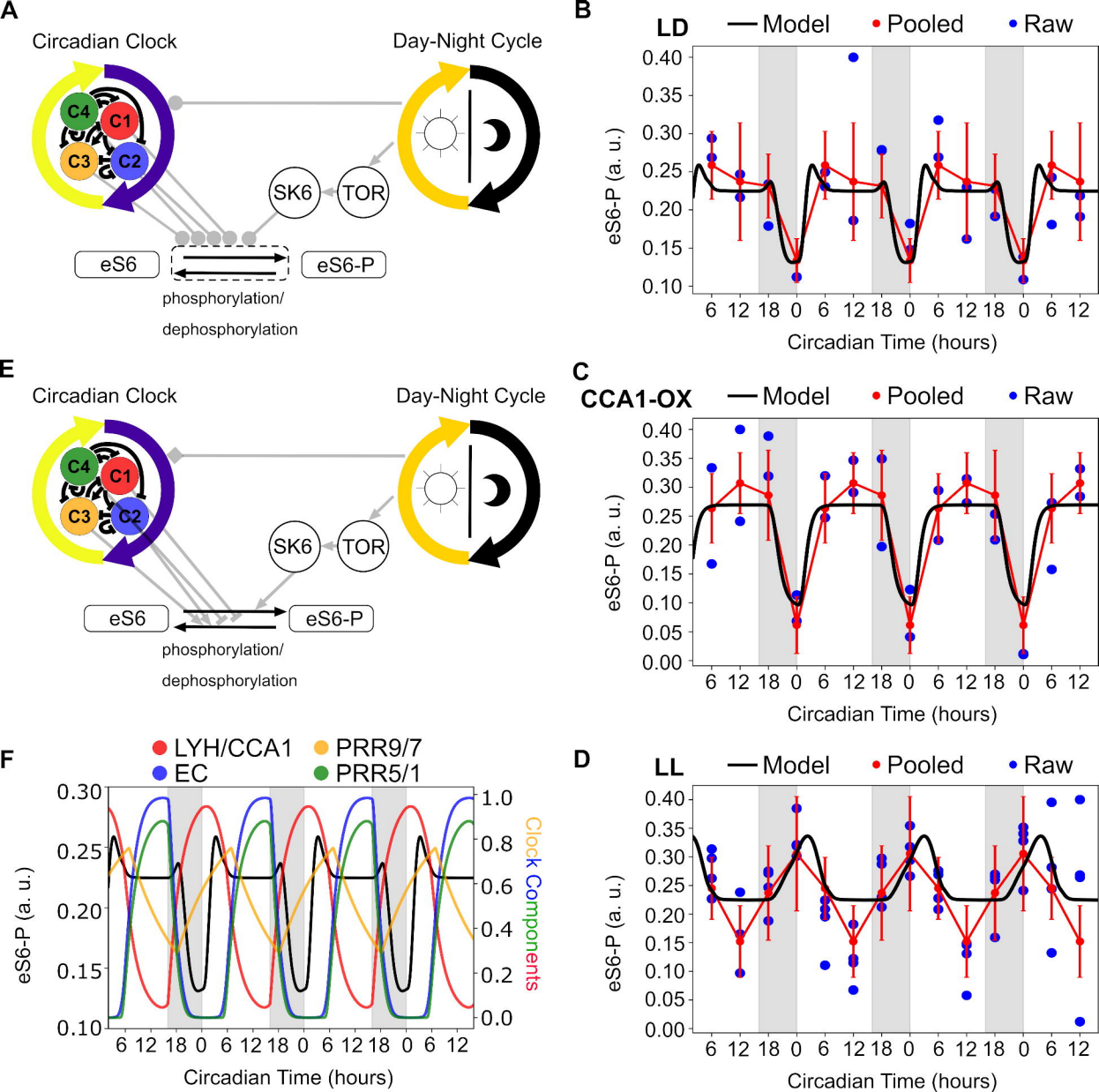
A
Circadian Clock
Day-Night Cycle
C4
C1
C3
C2
SK6
TOR
eS6
eS6-P
phosphorylation/
dephosphorylation
B
LD
Model
Pooled
Raw
eS6-P (a. u.)
Circadian Time (hours)
E
Circadian Clock
Day-Night Cycle
C4
C1
C3
C2
SK6
TOR
eS6
eS6-P
phosphorylation/
dephosphorylation
C
CCA1-OX
Model
Pooled
Raw
eS6-P (a. u.)
Circadian Time (hours)
F
LYH/CCA1
PRR9/7
EC
PRR5/1
eS6-P (a. u.)
Clock Components
Circadian Time (hours)
D
LL
Model
Pooled
Raw
eS6-P (a. u.)
Circadian Time (hours)

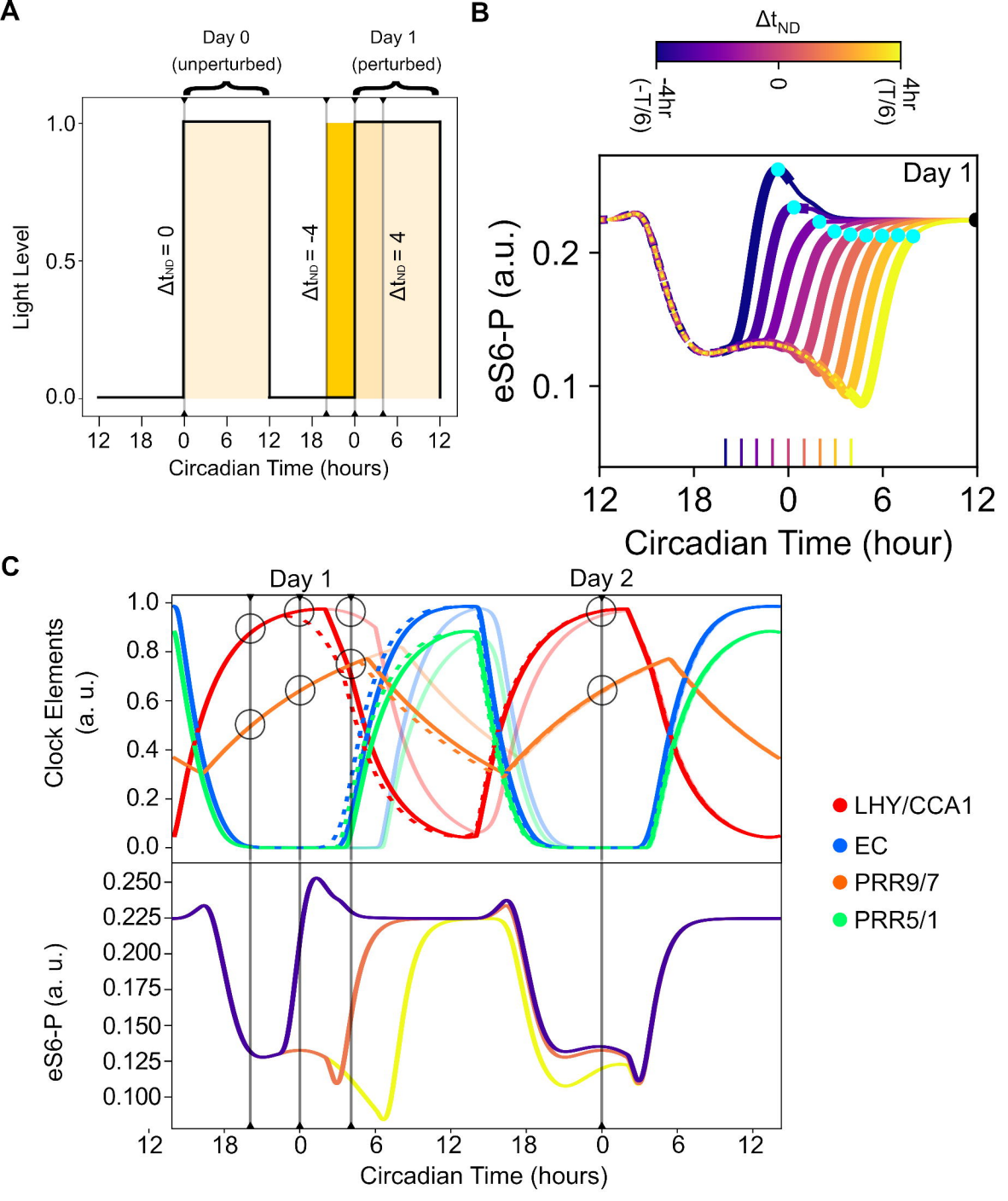
A
Day 0
(unperturbed)
Day 1
(perturbed)
Light Level
1.0
0.5
0.0
Δt_ND = 0
Δt_ND = -4
Δt_ND = 4
12 18 0 6 12 18 0 6 12
Circadian Time (hours)
B
Δt_ND
-4hr
(-T/6)
0
4hr
(T/6)
Day 1
eS6-P (a.u.)
0.2
0.1
12 18 0 6 12
Circadian Time (hour)
C
Day 1
Day 2
Clock Elements
(a. u.)
1.0
0.8
0.6
0.4
0.2
0.0
LHY/CCA1
EC
PRR9/7
PRR5/1
eS6-P (a. u.)
0.250
0.225
0.200
0.175
0.150
0.125
0.100
12 18 0 6 12 18 0 6 12
Circadian Time (hours)

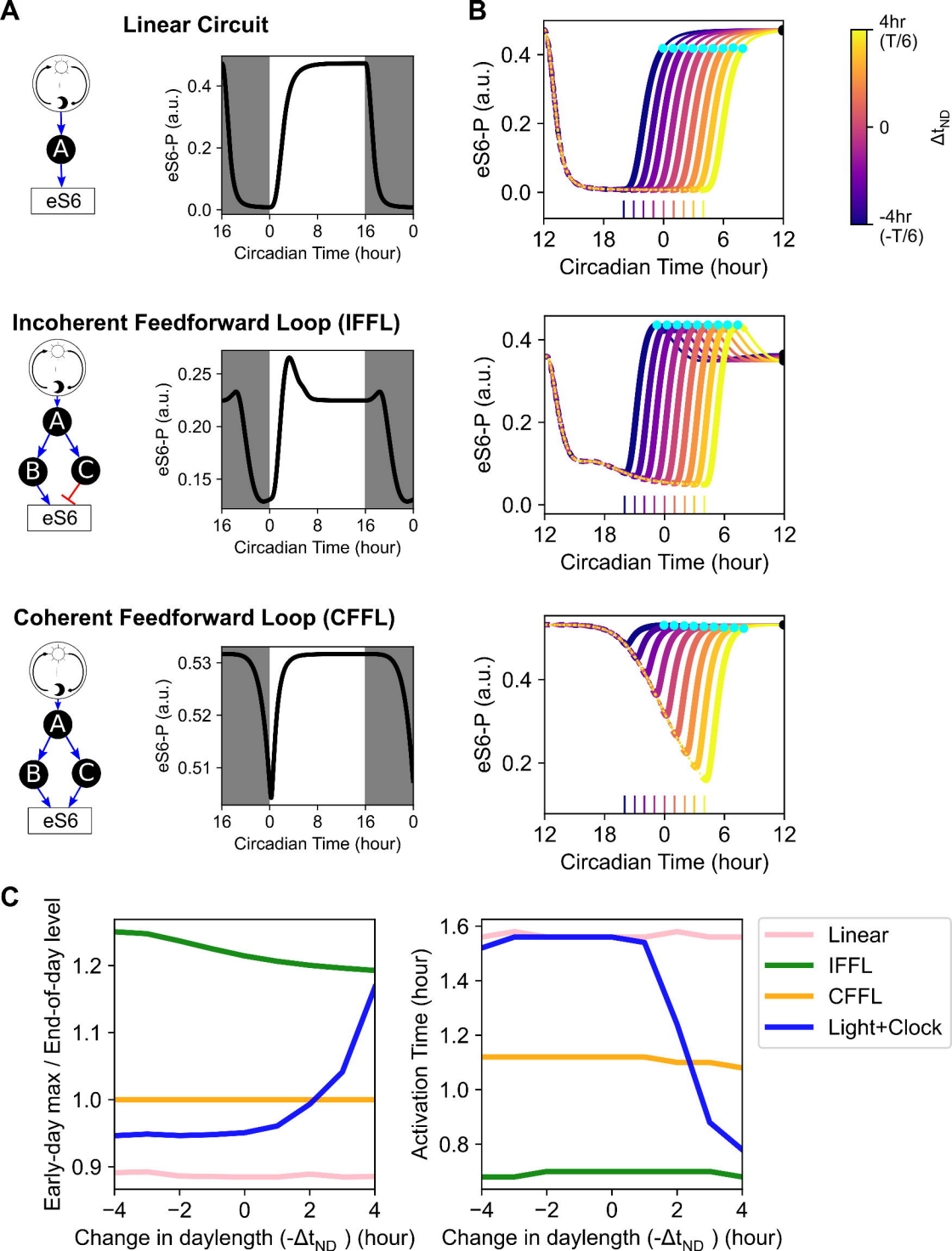
A
Linear Circuit
A
eS6
eS6-P (a.u.)
Circadian Time (hour)
B
4hr (T/6)
0
-4hr (-T/6)
Δt_{ND}
Incoherent Feedforward Loop (IFFL)
A
B
C
eS6
Coherent Feedforward Loop (CFFL)
C
Early-day max / End-of-day level
Activation Time (hour)
Change in daylength ($-\Delta t_{ND}$) (hour)
Linear
IFFL
CFFL
Light+Clock

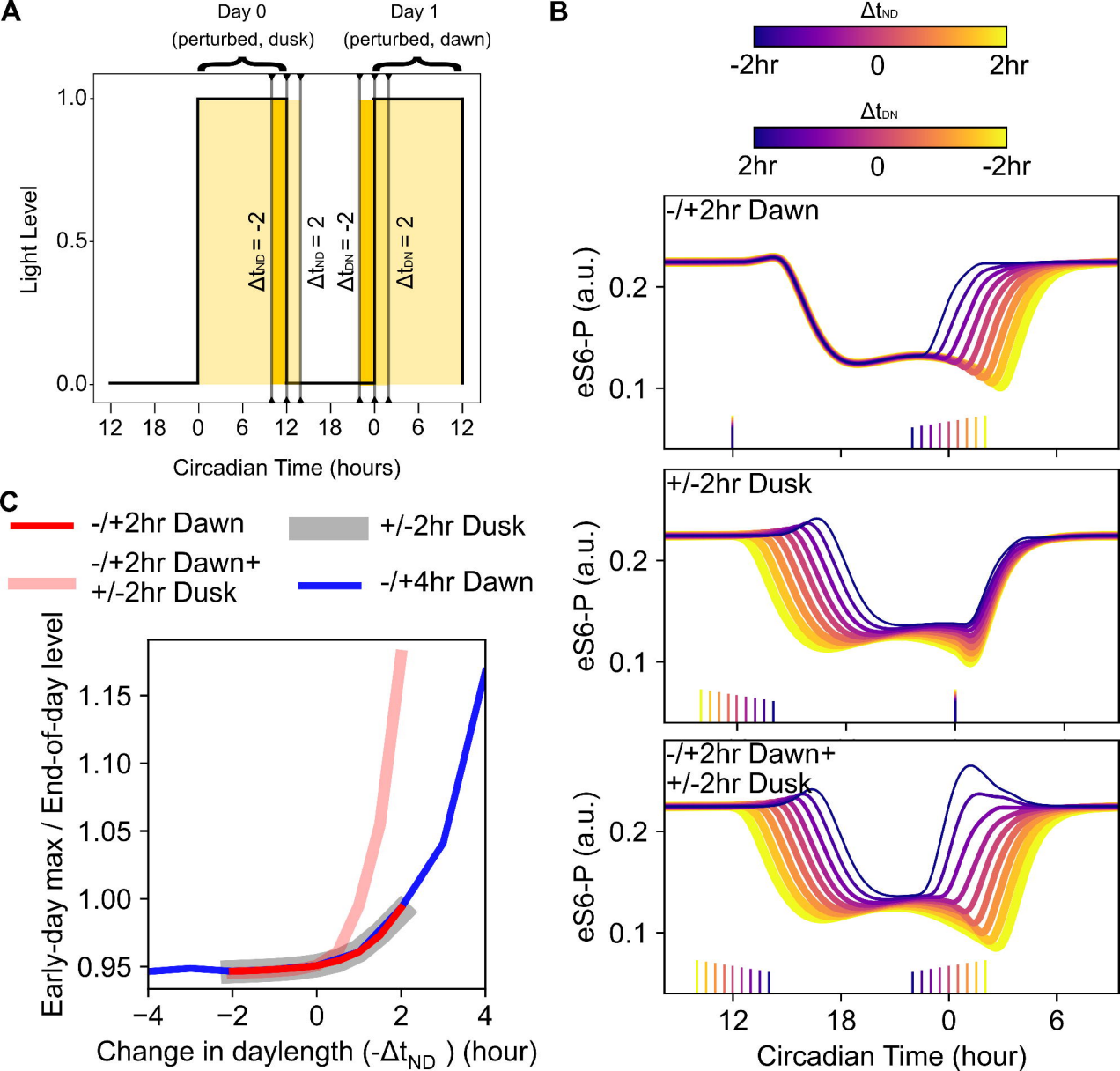
A
Day 0
(perturbed, dusk)
Day 1
(perturbed, dawn)
Light Level
1.0
0.5
0.0
Δt_ND = -2
Δt_ND = 2
Δt_DN = -2
Δt_DN = 2
12 18 0 6 12 18 0 6 12
Circadian Time (hours)
B
Δt_ND
-2hr 0 2hr
Δt_DN
2hr 0 -2hr
-/+2hr Dawn
+/-2hr Dusk
-/+2hr Dawn+
+/-2hr Dusk
eS6-P (a.u.)
0.2
0.1
12 18 0 6
Circadian Time (hour)
C
-/+2hr Dawn
+/-2hr Dusk
-/+2hr Dawn+
+/-2hr Dusk
-/+4hr Dawn
Early-day max / End-of-day level
1.15
1.10
1.05
1.00
0.95
−4 −2 0 2 4
Change in daylength (-Δt_ND) (hour)

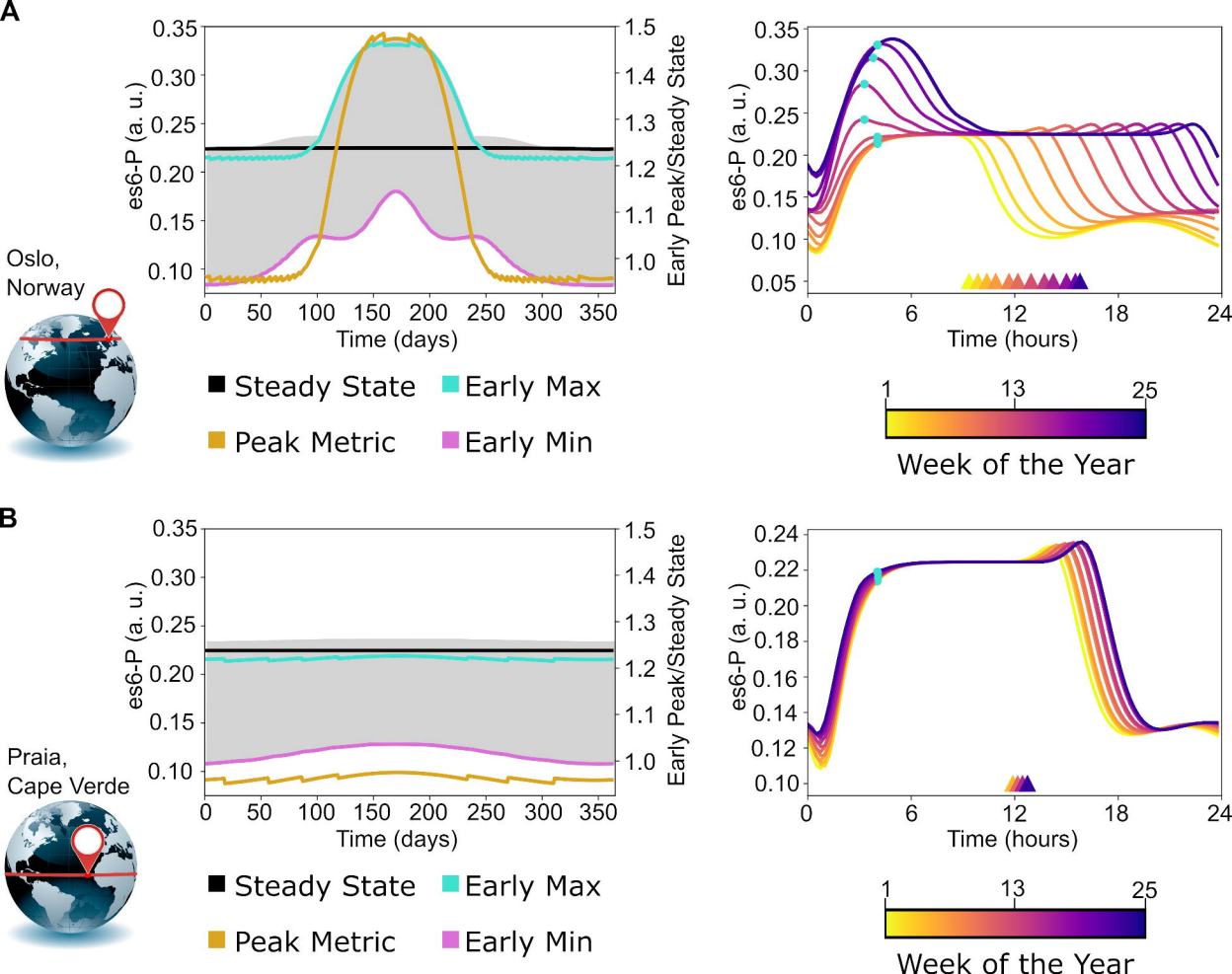
A
Oslo,
Norway
es6-P (a. u.)
Early Peak/Steady State
Time (days)
Time (hours)
Steady State
Early Max
Peak Metric
Early Min
Week of the Year
B
Praia,
Cape Verde
es6-P (a. u.)
Early Peak/Steady State
Time (days)
Time (hours)
Steady State
Early Max
Peak Metric
Early Min
Week of the Year

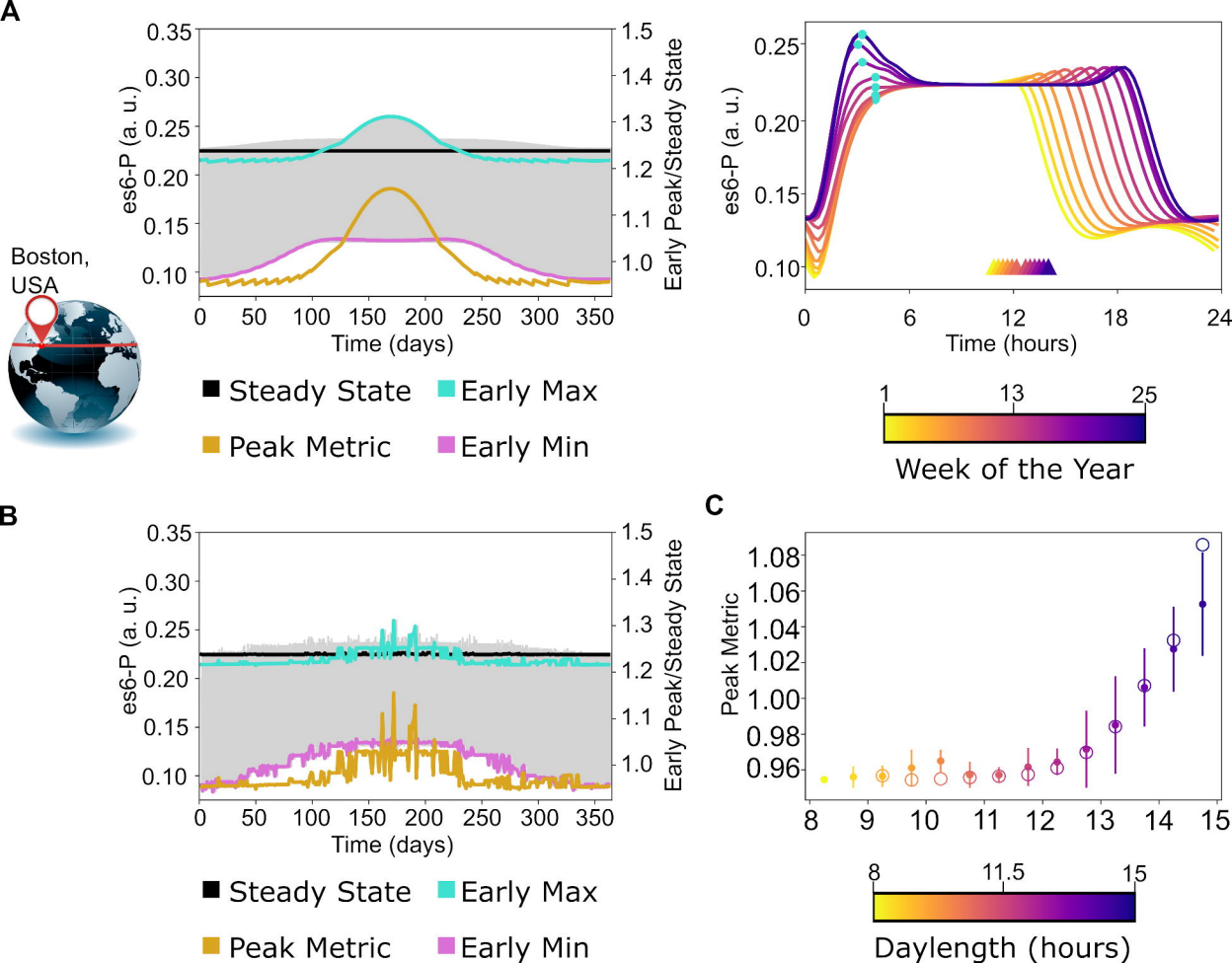
A
Boston, USA
es6-P (a. u.)
Early Peak/Steady State
Time (days)
Steady State
Early Max
Peak Metric
Early Min
Time (hours)
Week of the Year
B
C
Peak Metric
Daylength (hours)

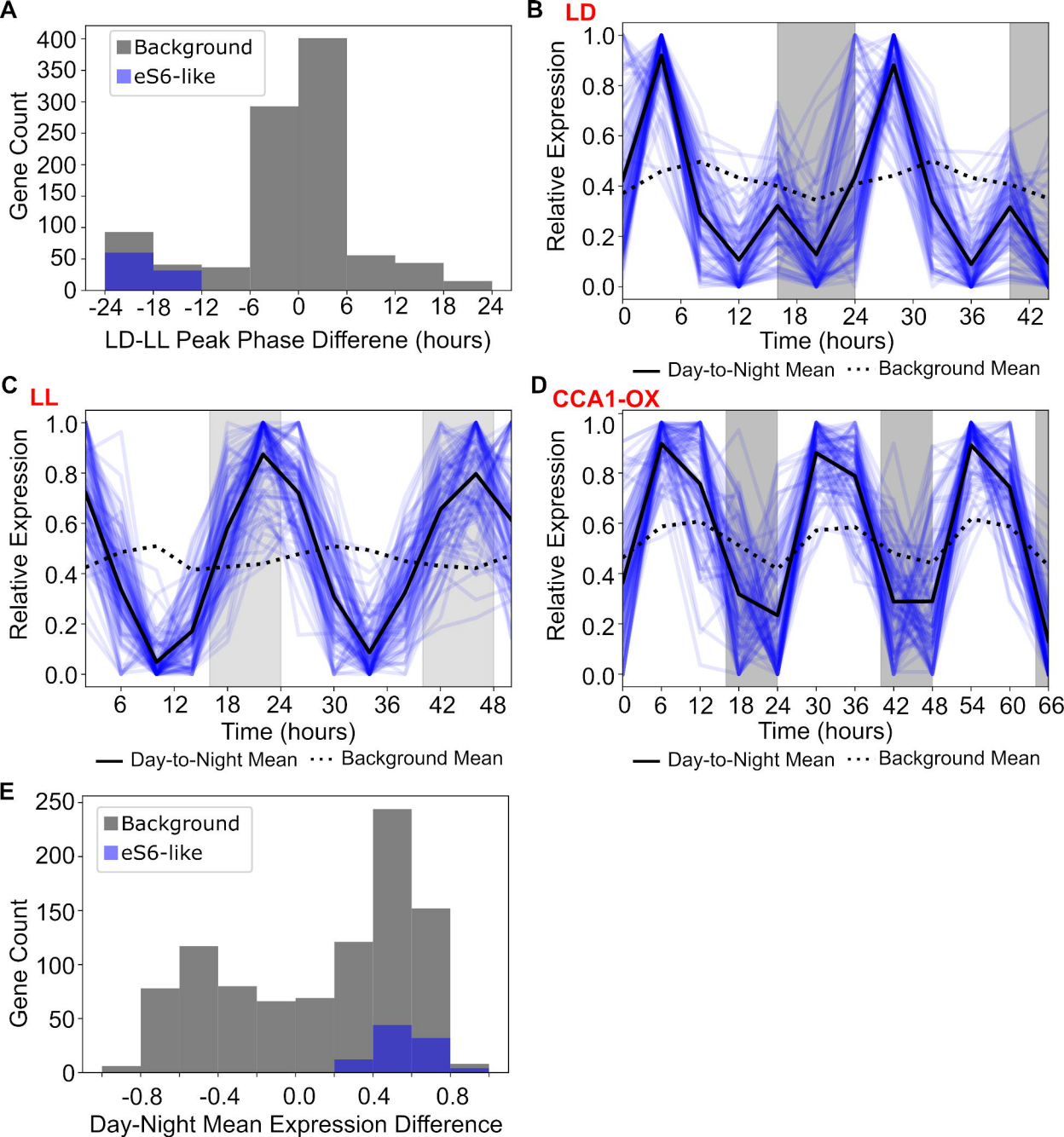
A
Background
eS6-like
Gene Count
LD-LL Peak Phase Differene (hours)
B
LD
Relative Expression
Time (hours)
Day-to-Night Mean
Background Mean
C
LL
Relative Expression
Time (hours)
Day-to-Night Mean
Background Mean
D
CCA1-OX
Relative Expression
Time (hours)
Day-to-Night Mean
Background Mean
E
Background
eS6-like
Gene Count
Day-Night Mean Expression Difference